INTERPRETATION OF VOLCANIC CONE PATTERNS IN THE ROYAL SOCIETY RANGE, TRANSANTARCTIC MOUNTAINS, USING A GIS APPROACH

A Thesis submitted for partial fulfillment
of requirements for the degree Bachelor of Science
in the Department of Geological Sciences
of The Ohio State University

Janna Kae Teets
Spring, 2004

Approved By 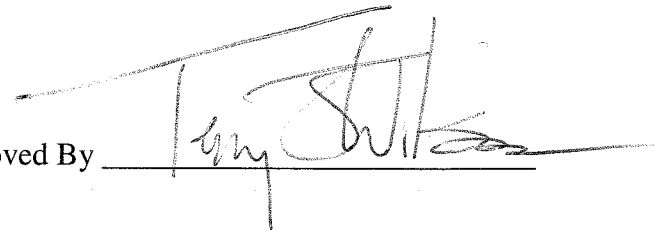

Dr. Terry J. Wilson

INTERPRETATION OF VOLCANIC CONE PATTERNS IN THE ROYAL SOCIETY RANGE, TRANSANTARCTIC MOUNTAINS, USING A GIS APPROACH

INTRODUCTION

As "manifestations of the ongoing structural evolution of the earth's surface," stress regimes provide important insight into the earth's geologic history and its current state (Bell, 1996a). Orientations of the principal horizontal stresses (S_{Hmin}, S_{Hmax}) acting on the earth's surface are related to the relative motions of tectonic plates and their geometries (Bell, 1996a). Past stress regimes offer information about the ways in which rocks, at one time, responded to the forces that acted on them, the presence of pore-fluid pressure, and their own mechanical properties (Bell, 1996b). Also, contemporary stress regimes shed light on present geological deformation processes and the way they respond to man-made activities, such as borehole drilling, mining excavations, and the extraction of solids and fluids (Bell, 1996b). This information can also aid in earthquake risk assessment and in the prediction of hydraulic fracture initiation and propagation direction.

Efforts have been made to compile contemporary global stress data (Zoback, 1992). The World Stress Map (WSM) project, initiated in 1986, is one such effort whose focus has been to describe intraplate stress fields, as opposed to those along the plate boundaries. Founded under the support of the International Lithosphere Program, its digital database currently consists of more than 7,300 *in situ* stress orientations. The WSM utilizes four different groups of geological and geophysical stress indicators to determine tectonic stress information: "earthquake focal mechanisms (63%), well bore breakouts and drilling induced fractures (23%), *in-situ* stress measurements (overcoring, hydraulic fracturing, borehole slotter (9%), and young [Quaternary] geologic data (from fault slip analysis and volcanic vent alignments (5%)" (http://www.world-stress-map.org). Zoback and Zoback (1989) developed a quality ranking system, defined by the letters A-E, to evaluate the accuracy of the recorded stress fields and to allow comparison of stress field orientations that have been gathered from differing sources (Zoback, 1992). It is as follows: A: orientation of S_H within ± 10-15°, B: orientation of S_H within ± 15-20°, C: orientation of S_H within ± 25°, D: questionable, E: recorded for completeness but not used (Zoback, 1992). Within the WSM database, earthquake and breakout stress indicator data account for approximately 85-90% of the A-C quality data.

Within Antarctica almost no stress data exists because few earthquakes have been recorded and no commercial drilling has taken place. Yet, Antarctica is home to widespread Cenozoic volcanic provinces, which provide an opportunity to use volcanic alignments as a means to map Cenozoic stress fields (Kyle, 1990).

This study forms part of a project known as the "Antarctic Stress Map Project (ASMAP)" with the focus of mapping the stress patterns in the McMurdo Volcanic Province (Figure 1, Kyle 1990), and is funded by the Office of Polar Programs, National Science Foundation, to T. Wilson, The Ohio State University, and T. Paulsen, The University of Wisconsin-Oshkosh. The objectives of this study are to compile age data for Cenozoic volcanic rocks in the Transantarctic Mountains (TAM), use the map of volcanic cones in the TAM to interpret alignment trends, and to correlate volcanic alignments with age data to determine if there are one or more stress directions defined by the alignments in the TAM.

EREBUS VOLCANIC PROVINCE: SETTING OF THE STUDY AREA

The McMurdo Volcanic Group has been divided into three provinces according to tectonic setting, spatial distribution, and possible petrologic variations (Kyle, 1990). The Erebus volcanic province is the most studied, and therefore, the most geologically known (Figure 2, Kyle 1990). The still active volcano, Mt. Erebus, contains a "lava lake of anorthoclase phonolite magma" driven by convection, with bombs being ejected onto the crater rim daily by strombolian eruptions (Kyle, 1990). The majority of volcanism in this province is contained in the Ross Island and the Discovery subprovinces. Magnetic surveys and seismic profiling also show large regions of volcanic rocks beneath the Ross Sea, especially in the western portions. Within the Erebus volcanic province, most vents are underlain by thinned crust within the area covered by the Ross Sea and the Ross Ice Shelf known as the "Ross Embayment" (Kyle, 1990). This part of the Ross Embayment is underlain by the Victoria Land rift basin, which contains over 12 km of sediment (Figure 3, Kyle 1990).

Armstrong (1978) and Wright-Grassham (1988) used the K-Ar method to determine many radiometric ages from surface samples from the Erebus volcanic province, the oldest being 19 m.y. old (Kyle, 1990). At about 4 Ma, volcanism in the area became more widespread and Ross Island became more "built up" with the formation of Mount Bird (4-3 Ma), Mount Terror (2-0.6 Ma), Hut Point Peninsula (1.8-0.4 Ma), and Mount Erebus (<1 Ma) (Kyle, 1990). Kyle (1979) used the classification suggested by Coombs and Wilkinson (1969) to describe the volcanic rocks in the Erebus volcanic province. The majority of the lavas belong to the basanite, phonolite, and trachyte fields, with intermediate compositions. Many xenoliths have also been found in the province that contain the "composition of the lithosphere and processes which have affected it," including "supracrustal material, mafic and felsic granulites, and a wide range of mafic and ultramafic types" (Kyle, 1990).

The volcanic vents investigated in this study are concentrated within the eastern foothills of the Royal Society Range of the TAM within the Erebus volcanic province (Figures 1 & 4; Kyle, 1990; Wright and Kyle, 1990). The mountain area itself is a 70 km wide rift-flank block adjacent to the Victoria Land rift basin, and is part of the "upward margin of an extensive landsurface that rises gradually from the interior of Antarctica and eventually emerges from beneath the East Antarctic Ice Sheet" (Sugden, 1999). The altitude along its rim is approximately 3000 m, with Mt. Lister as its highest peak (4025 m above sea level) (Sugden, 1999). A large rift-margin escarpment 1600-2000 m high lines the coastal trace. The relief of the Royal Society Range is one of the highest of any passive continental margin (Sugden, 1999).

A Precambrian igneous and metamorphic basement constitutes the exposed bedrock of the Royal Society Range. Devonian to Triassic age siltstones, sandstones, and conglomerates unconformably overlie the Precambrian bedrock (Sugden, 1999). The main types of volcanism in the area are cinder cones and lava flows that are located between the Royal Society Range and the Koettlitz Glacier (78°04'-78°26'S, 162°35'164°20'E) (VAP, 1990). Over 50 vents are found here, and range from small scoria mounds to larger cones up to 300 m in height that are often intruded by dikes and composed of "intercalated scoria, agglutinate, bombs, and lava flows" (Kyle, 1990). The majority of the lava flows are less than 4 km long, and are usually 30-100 cm thick within the cones and 3-10 m thick extending outside the cones. Most of the rocks in the Royal Society Range are porphyritic basanites with varying amounts of olivine and clinopyroxene phenocrysts and small amounts of opaque minerals and phenocrystic plagioclase (Kyle, 1990). Wilch (unpublished report) used $^{40}Ar/^{39}Ar$ age data from the Southern Foothills of

the Royal Society Range to define 39 "basaltic eruptions that occurred in isolated pulses during the Miocene," and during 30 episodes since 2.5 Ma (Figure 5, Wilch).

STRESS DIRECTION FROM VOLCANIC CONE AND FISSURE ALIGNMENTS

The volcanic cone and fissure alignments mapped in the Royal Society Range study area serve as regional stress field indicators. Where volcanic cones form alignments in the form of linear clusters of circular or elongate cones, they are interpreted as being located above linear volcanic fissures and extension fractures, which served as a conduit for the feeding of magma up to the earth's surface (Adiyaman, 1998; Figure 6). Due to the regional stress field on the surface of the earth, these alignments will form normal to the least compressive stress or the greatest tensile stress acting on the earth's crust if they form in an isotropic rock. However, the ascending magma could also follow pre-existing faults or fractures in the intruded rock, and not necessarily be controlled by the regional stress field.

According to Adiyaman (1998), Nakamura (1969) first proposed the use of volcanic cones as tectonic stress regime indicators, and Jackson and Shaw (1975) used the Hawaiian-Emperor system in the Pacific to show that linear volcanic chains indicate stress trajectories (σ_1 and σ_2). Nakamura (1977) again proposed that radial dike patterns of volcanic cones could be used to resolve the orientation of tectonic stresses. His findings revealed that the direction of dike propagation across a volcano paralleled the maximum horizontal compressive stress (σ_{Hmax}) and formed alignments of flank volcanic eruptions on polygenetic volcanoes (Tibaldi, 1995). Because regional stresses influence the orientation of dikes, and flank volcanic eruptions on the slopes of polygenetic volcanoes act as a surface manifestation of radial dike patterns, the distribution of flank volcanic eruptions can be used to determine the orientation of regional stresses (Figure 7, Nakamura 1977).

Radial dike patterns develop when the stress field is isotropic or when low differential stress is present (Figure 8). This occurs when either the magmatic pressure within the central conduit is greater than other stresses, or the stresses do not differ in horizontal direction (Nakamura, 1977). The flank eruptions that form as a result of radial dikes are mainly monogenetic; they erupt only once causing a new magma feeder conduit to develop with every eruption. As seen in Figure 7 (Nakamura, 1977), radial dike orientations may be used to determine the regional trajectories of the maximum and least compressive stresses (σ_1 and σ_3). The shape and distribution of dike patterns also give information about tension fractures that directly relate to the tectonic regime. If the stress field is highly differentiated, that is, if the maximum horizontal compressive stress (σ_{Hmax}) is significantly greater than the least horizontal compressive stress (σ_{Hmin}), then an hourglass dike pattern develops (Figure 8). Here, σ_{Hmax} is orientated parallel to the long axis of the volcanic cone and the superposed volcanic alignments, and σ_{Hmin} is oriented perpendicular to the long axis.

Dikes form parallel to the plane defined by the maximum and intermediate stress axes (σ_1 and σ_2), and are mainly vertical in cross-section. With one of the principal stress axes assumed to be vertical, and the other two horizontal at the surface of the earth, the trend of the zone of flank eruptions is in the direction of the maximum or intermediate compressive principal stress axes. The latter case relates to extensional tectonics, and the former to contractional tectonics (Nakamura, 1977). In an entire volcanic zone, the formation of a new magma conduit in a monogenetic volcano is much easier in extensional tectonics, than in contractional tectonics,

where magma can most easily rise through a pre-existing system. The azimuthal direction of flank eruptions tends to be distributed around the trend of the maximum horizontal compressive regional stress. The direction of the minimum compressive stress is oriented close to the ambient stress that is perpendicular to the trend of the flank eruption zone. This is due to the very low tensile strength of the surrounding rocks due to high temperatures, which is effective only at the time of the dike formation (Nakamura, 1977).

The basis of dikes as stress indicators is magmatic hydrofracture, which occurs where magmatic pressures exceed the compressive stress acting on a dike plane, generating tension in the rock body that extends farther beyond the dike tip (Delaney, 1986). This tension may be large enough to propagate a new fracture into which magma could flow. In this case, dike propagation is in a plane perpendicular to the least compressive stress, thus indicating principal paleostress directions. However, in tectonically inactive regions, dikes may exploit pre-existing joints without a preferred orientation (Delaney, 1986). In this case, dike orientations are not sufficient indicators of principal stress directions. If the dikes are of the same age and have different strikes, then it can be concluded that the stress state at the time of formation was heterogeneous, or that they were not affected by the direction of least compressive regional stress. These dikes would not be useful indicators of paleostress orientations (Delaney, 1986). If the strikes are similar, then it is possible that other tectonic features with the same strike acted as "planes of weakness" for the magma.

When analyzing the orientations of dike patterns, certain assumptions and ambiguities arise that can either help or hinder the analysis process. For example, one may have to assume that a line of cones that seem to belong to the same linear feature are in fact a true linear feature, not just a random pattern. To define alignment patterns, specific criteria need to be used. First, the line running through the long axis of a single elongate cone or a series of elongate cones may define an alignment. Also, an alignment may be defined by a line connecting the midpoints of a string of circular cones, or by the "best fit" line through a linear cluster of circular cones. Parameters also have to be set to define the limits of lineaments, such as where one alignment ends and where another begins. It is up to the analyst to define what makes up a linear feature and what cones can be grouped together when examining cone orientations. However, every analyst is different, and what might seem like a linear pattern to one might not seem the same to another. Thus, ambiguities may arise while attempting to distinguish cone alignment features.

In addition to the above criteria, the ages of the cones have to be known so that interpretations of the stress regimes can be made for different geologic times. For example, cones of a known similar age that form a linear cluster could surely be interpreted as being subject to the same regional stress at the time of formation. The ages of alignments can be measured by absolute dating of the volcanic cones, and by crosscutting relations. Absolute dates provide information about the stress field at definite geologic times, whereas crosscutting relations provide relative ages for ancient stress fields. Overall, the recognition of volcanic cone alignment features should be analyzed with the above assumptions and ambiguities in mind.

Breaching is another feature of volcanic cones that provides information on the orientation of the fracture that fed magma to the cone, and it seems to be due to the magmatic intrusion into a pre-existing cone (Tibaldi, 1995). In fault-strike breaching, the direction of breaching parallels the underlying fault, points in the downslope direction, and may be caused by the weakening of the two sides normal to the fault due to hydrothermal activity, fault propagation, or lava propagation. The other direction of breaching occurs perpendicular to the trend of fault-strike breaching and corresponds to the fault dip direction of underlying normal

faults. It is known as fault-dip breaching (Figure 9, Tibaldi 1995). In this case, breaching may be due to the presence of an escarpment in the underlying fault oriented in the same direction, or to the presence of dikes parallel to the strike of the fault. It was found that within the cones a relative increase in the magnitude of the stress occurred in the direction of breaching. This increase was initiated when the magma ascended to the cone base and then "grew geometrically" while following a preferred path until breaching occurred (Tibaldi, 1995).

GIS FOR THE ROYAL SOCIETY RANGE SECTOR OF THE EREBUS VOLCANIC PROVINCE

Existing GIS

A Geographical Information System (GIS) is a computer-based capability for the manipulation of geographical data. The GIS software used in this study was ArcView 3.2, which enables its users to "visualize, explore, query, and analyze data geographically" (ArcView, 1996). Within a GIS, spatial information is presented in two ways; as vector data in the form of points, lines, and areas (polygons); or as grid data in the form of uniform, systematically organized cells. Another format for storing spatial data in a GIS is in an image file, in which spatial information in an image is stored within pixels (grid cells), and are drawn "as-is" within ArcView. The images used in this study were scanned maps and satellite imagery.

Several elements were provided for the GIS aspect of this project. A topographic base map was downloaded from the United States Antarctic Resource Center (http://usarc.usgs.gov/) and a Landsat image of the area was provided by T. Wilson from the "Antarctic Stress Map" research project (ASMAP). A "vector layer" was provided for this study containing the outlines of volcanic scoria cones, related flows, and dikes that were mapped by T. Wilson and T. Paulsen from satellite imagery, aerial photographs, and in the field.

Compilation of Age Data for Volcanic Rocks in the GIS

A major contribution of this study was to compile all available age data for the volcanic rocks in the Royal Society Range area into the GIS. For the Royal Society Range study area, four different data sources were used to map the ages of the volcanic rocks [Armstrong (1978), Wright and Kyle (1990), Sugden (1999), Wilch (unpublished report)]. The Armstrong (1978) data set did not contain a map, but rather, a data table with latitude/longitude coordinates for the cones that had been determined from 1:250,000 scale topographic maps. It also contained K-Ar dates for the volcanics obtained using analytic techniques and decay constants current in the 1970s. To bring these ages up to date, they were recalculated using new decay constants (Appendix A). The Wright and Kyle (1990) data set contained a sketch map with outlines of volcanic outcrops, with no distinction made between scoria cones, lava flows, and dikes (Appendix B). Indistinct sample locations on the map were connected by a line to a box containing one or more age dates (Figure 4, Wright and Kyle 1990). The Sugden (1999) data set included a sketch map with dots marking volcanic cone locations, some of which were paired with an age date (Figure 10; Appendix C). The extent of volcanic outcrops is not shown on the map. The Wilch (unpublished report) data set contained two sketch maps, one showing numbered circles representing sample locations referenced to a table, and the other showing outlines of volcanic outcrops, with no distinction made between scoria cones, lava flows, and

dikes, connected by a line to a box containing one or more age dates (Figures 11 & 12). Wilch provided new Ar-Ar dates for the volcanic rocks, and a table matching the ages of his samples to the Armstrong (1978) samples, where the same volcanic units were dated.

The next task was to correlate the age dates by identifying the ones that were repeated on more than one map and those that were unique. The three source maps from Wilch (unpublished report), Wright and Kyle (1990), and Sugden (1999) were scanned, and the given coordinates were used to rectify the maps into a common projection within the ArcView GIS. The Armstrong (1978) coordinates for the dated volcanic samples were then typed into an ASCII file, loaded into ArcView, and put into the same projection. These ages were entered as a "point theme," a data layer in ArcView that represents the geographical locations of the age dates as points. For the Wilch (unpublished report), Wright and Kyle (1990), and Sugden (1999) data sources, separate point themes for the ages on each source map were created in ArcView by digitizing each age location from the maps, allowing the age locations provided by each source to be represented digitally within ArcView. Difficulties arose while creating the point themes for the Wilch (unpublished report) and Wright and Kyle (1990) maps where age dates were connected by lines to volcanic outcrops. It was assumed that the sample locality was located at the end of the visible black line, however, in some cases, this was obscured because the black line was overlain on a volcanic outcrop displayed as black on the map. The locations for the sample localities were best estimated. On the Wilch (unpublished report) and Wright and Kyle (1990) maps, where two age dates pointed to the same location, two points were added as closely as possible without putting one directly on top of the other.

Next, the age data for each source had to be matched to each other. When two or more of the point data sets were overlain using ArcView, many age points were close together, but not exactly in the same location; overlaying the point themes could not unambiguously match the same age points. This was due to errors introduced by the initial photocopying, scanning, and projecting of the maps into ArcView, by the fact that the sketch maps were not accurate base maps, by the inaccuracies in the Armstrong (1978) coordinates that were originally read from 1:250,000 scale topographic maps, and by the ambiguities in digitizing the age locations from the source maps. At this stage it was only possible to remove some of the redundant age data by comparing point locations and by comparing age values. If point locations were close and the ages matched, the dates were considered to be the same. It was found that Wright and Kyle (1990) used Armstrong age dates, but it was not known which ages were from Armstrong (1978) and which were from other sources. To sort this out, the point themes for Armstrong (1978) and Wright and Kyle (1990) were overlain, and points were found that matched closely in space and where Armstrong (1978) and Wright and Kyle (1990) ages were the same. The Armstrong (1978) ages were retained in the data set, and the Wright and Kyle (1990) data was revised to consist only of ages from other sources. An unpublished report was received from Wilch with maps and tables for the age date samples, which were the original data for the Sugden (1999) map, so the Sugden (1999) data source was discarded and the Wilch (unpublished report) data was used instead. Armstrong (1978) K-Ar age dates were also eliminated that proved to be the same volcanics dated by Ar-Ar by Wilch (unpublished report) using his correlation table. The new age data from Wilch (unpublished report) was used for these localities.

The next step was to match the age data to the mapped outlines of volcanic scoria cones, related flows, and dikes for the purpose of stress interpretation. The ASMAP project map of volcanic dikes, cones, and flows for the study area was compared to the aerial photographs and imagery from Wilch (unpublished report) to match the age date locations to the mapped cones,

alignments were dated by 16 Wilch and 0 Armstrong data points. The 2 probable alignments trend N14E and N66W, and the 8 possible alignments trend N20E, N21E, N33E, N44E, N58E, N84E, N75W, and N83W.

Age of Alignments

The ages of the alignments that were used in this study naturally fall into 3 main groupings of young, middle-aged, and older alignments, more specifically, 0.196 Ma to 2.57 Ma, 4.26 Ma, and 11.34 Ma to 14.58 Ma. Thirty-nine dated sample points from Wilch (35) and Armstrong (4) were used in this project to interpret alignment patterns from dikes, elongate cones, and strings of circular cones that form a linear pattern. Other dated samples from each of these sources were too inconclusive or ambiguous to accurately deduce such patterns. Chart 1 lists the interpreted alignments with their ID's, dates, date sources, trends, alignment indicators, quality, and remarks.

The younger alignment group as a whole consists of 23 alignments. Eight of the eleven dike alignments are within the younger-aged group, and are dated by 10 Wilch and 2 Armstrong data points. Dike D1, located in the northwestern section of the study area, trends N23E and is dated by W19 and W20 at 1.62 and 1.6 Ma, respectively. D2 trends N46W and is dated by W23 at 1.91 Ma. D3, the westernmost dike alignment, trends N43W and is dated by W25 and W26 at 0.32 Ma and 0.28 Ma. D4, located in the central section, trends N49E and is dated by W30 and W31 at 0.981 Ma and 1.21 Ma. D5 trends N14E, and is dated by W37 at 2.505 Ma. D6 trends N85E and is dated by W46 at 1.9 Ma. D7, located in the southeastern section of the study area, trends N19E and is dated by W48 and A47 at 1.261 Ma and 1.66 Ma. D8, also in the southeast, trends N17E and is dated by A54 at 1.65 Ma. Overall, six of the younger dike alignments trend northeast and two trend northwest.

All seven alignments defined by the long axis of elongate cones are within the younger group of alignments, and are dated by 6 Wilch and 2 Armstrong data points. Elongated cone EC1, located in the northwestern section of the study area, trends N33E and is dated by sample W47 at 0.271 Ma. EC2, located in the southwest, trends N2E and is dated by W22 at 0.853 Ma. Slightly southeast of EC2 is EC3, trending N1E and is dated by W21 at 1.065 Ma. In the southeast, EC4 trends N19E and is dated by A66 at 1.68 Ma. EC5 trends N27E and is dated by W58 and A65 at 1.99 Ma and 2.44 Ma, respectively. EC6, located in the northwest and aligned with an undated elongated cone slightly to the north, trends N20E, and is dated by W29 at 2.08 Ma. EC7 trends N3W and is dated by W8 at 2.57 Ma, the uppermost age limit for the younger alignment group. Overall, six of the younger alignments defined by the long axes of elongated cones trend northeast, and one trends northwest.

Eight of the ten alignments defined by 2 or more circular cones with a linear trend are within the younger group of alignments, and are dated by 16 Wilch and 0 Armstrong data points. Chart 1 lists in further detail the evidence obtained to support these alignments. Circular cone alignment CC1, located in the western section of the study area, trends N20E and is dated by sample W41 at 0.196 Ma. CC2, located northeast of CC1, trends N84E and is dated by W36 at 1.08 Ma. CC3 trends N33E and is dated by W28 at 1.14 Ma. CC4, the southwestern most alignment in the study area, trends N44E and is dated by W57 at 1.17 Ma. CC5 trends N75W and is dated by W16, W17, and W18 at 1.55 Ma, 1.37 Ma, and 1.769 Ma respectively. CC6 trends N83W and is dated by W24 at 1.63 Ma. CC7, located in the central section of the study area trends N58E and is dated by W2, W3, and W4 at 2.17 Ma, 1.925 Ma, and 1.877 Ma,

respectively. CC8 trends N14E and is dated by W35 and W38 at 2.534 Ma and 2.28 Ma. Of all these alignments, CC1 through CC7 are possible and CC8 is probable. Overall, six of the younger alignments defined by circular cones trend northeast, and two trend northwest.

The younger alignment group contains 12 definite, 1 probable, and 5 possible alignments that trend northeast. It also contains 3 definite and 2 possible alignments that trend northwest. Therefore, the evidence strongly suggests that the best interpretation for this group ranging from 0.196 Ma to 2.57 Ma is a northeast trending alignment pattern.

Only one alignment falls in the middle-aged alignment group. This is a definite dike alignment D9 and is located in the far eastern section of the study area. It trends N18E and is dated by sample W6 at 4.26 Ma. No conclusive elongate cone or circular cone alignments were defined in this age range. The best interpretation for this middle-aged group is a northeast trending alignment pattern.

Two of the eleven dike alignments are within the older group. Dike alignment D10, located in the western section of the study area, trends N38E and is dated by sample W34 at 11.98 Ma. W7 is the easternmost interpreted alignment, trends N26E, and is dated by W7 at 14.58 Ma, the oldest age sample in this study. Both dike alignments are definite. Two of the ten alignments defined by 2 or more circular cones with a linear trend are within the older group, and are dated by 3 Wilch and 0 Armstrong data points. Circular cone alignment CC9, located near the northeastern corner of the study area, trends N66W and is dated by samples W10 and W33 at 11.34 Ma and 12.43 Ma, respectively. This is interpreted to be a probable alignment. CC10 is a possible alignment defined by a circular cone in close proximity to 2 more circular cones with a linear trend. It trends N21E and is dated by W32 at 12.1 Ma. Of the four older alignments, 3 trend northeast and 1 trends northwest.

Overall, the older group contains 2 definite alignment patterns that trend northeast, 1 probable alignment that trends northwest, and 1 possible alignment that trends northeast. This evidence suggests that the best interpretation for this group ranging from 11.34 Ma to 14.58 Ma is an alignment pattern trending northeast.

Stress Pattern(s)

The best interpretations for the alignment patterns of the 3 age groups described above and their supporting evidence indicate that the stress field for the study area did not change through time, that is, the stress field did not change from 0.196 Ma to 14.58 Ma. The interpretation for each age group is an alignment pattern that trends northeast. Because the maximum horizontal compressive stress (σ_{Hmax}) parallels the alignments, this indicates that σ_{Hmax} was also oriented in a northeast-southwest direction, and σ_{Hmin} was oriented in a northwest-southeast direction for the age range used in this study.

The scope of this study did not include determining whether the alignment patterns were controlled by pre-existing fractures. If it were, the alignment patterns of the dikes, elongated cones, and circular cones would have been compared to the alignment patterns of other geologic structures, such as, foliation, faults, and geologic contacts. If the interpreted alignments patterns paralleled these geologic alignments, then it could be interpreted that the alignments were controlled by pre-existing fractures.

Conclusions

The GIS approach utilized in this study was useful because it allowed the age data to be manipulated spatially and analyzed geographically within a map of the study area. Within ArcView, age data sets from several sources were able to be overlain and viewed together to determine matching data points and ones that were unique. While this did not lead to complete unambiguous data point matches, it did narrow the final data set to those points that were used in this study to date the alignment patterns of the mapped dikes, elongate cones, and circular cones.

Using the dated samples from the Wilch and Armstrong data sets, alignment patterns of the mapped dikes, elongate cones, and circular cones were measured and dated. The ages of the alignment patterns fell into 3 groups of younger, middle-aged, and older alignments, ore specifically, 0.196 Ma to 2.57 Ma, 4.26 Ma, and 11.34 Ma to 14.58 Ma. It was found that the best interpretation for each group was an overall alignment pattern trending northeast. This indicates a stress field within the study area that did not change through time, with the maximum horizontal compressive stress (σ_{Hmax}) oriented in a northeast-southwest direction, and the least horizontal compressive stress (σ_{Hmin}) oriented in a northwest-southeast direction.

References

Adiyaman, Ö. 1998. Relationships between volcanic patterns and neotectonics in Eastern Anatolia from analysis of satellite images and DEM. *In* Journal of Volcanology and Geothermal Research. Vol. 85. p. 17-32.

ArcView. 1996. Using ArcView GIS. Environmental Systems Research Institute, Inc.

Armstrong, Richard L. 1978. K-Ar dating: Late Cenozoic McMurdo Volcanic Group and dry valley glacial history, Victoria Land, Antarctica. *In* N.Z. Journal of geology and Geophysics. Vol. 21, No.6. p. 685-698.

Bell, J.S. 1996. Petro Geoscience 1. In Situ Stresses In Sedimentary Rocks (Part 1): Measurement Techniques. *In* Geoscience Canada. Vol. 23. No. 2. p. 85-100.

Coombs, D.S., and J.F.G. Wilkinson. 1969. Lineages and fractionation trends in undersaturated volcanic rocks from the east Otago volcanic province (New Zealand) and related rocks. *In* Journal of Petrology. Vol. 10, No. 3. p. 440-501.

Delaney, Paul T. 1986. Field Relations Between Dikes and Joints: Emplacement Processes and Paleostress Analysis. *In* Journal of Geophysical Research. Vol. 91. No. B5. p. 4,920-4,938.

Kyle, P.R., et al. 1979. Geology and petrology of the McMurdo Volcanic Group at Rainbow Ridge, Brown Peninsula, Antarctica. *In* Geological Society of America Bulletin. Vol. 90, No. 7. p. I 676-I 688. Geological Society of America (GSA). Boulder, CO.

Kyle, P.R. 1990. McMurdo Volcanic Group-Western Ross Embayment. *In* Volcanoes of the Antarctic Plate and Southern Oceans. Vol. 48. p. 18-139. American Geophysical Union. Washington, D.C.

Nakamura, K. 1977. Volcanoes As Possible Indicators Of Tectonic Stress Orientation-Priniple And Proposal. *In* Journal of Volcanology and Geothermal Research. Vol. 2. P. 1-16.

Sugden, David E., et al. 1999. Landscape development in the Royal Society Range, southern Victoria Land, Antarctica: stability since the mid-Miocene. *In* Geomorphology. Vol. 28. p.181-200.

Tibaldi, Alessandro. 1995. Morphology of pyroclastic cones and tectonics. *In* Journal of Geophysical Research. Vol. 100. No. B12. p. 24,521-24,535.

Wilch, Thom. Unpublished Report. $^{40}Ar/^{39}AR$ geochronology of Miocene to Late Pleistocene basaltic volcanism in the Southern Foothills of the Royal Society Range, South Victoria Land, Antarctica. University of Maine. Orono, ME.

Zoback, Mary Lou, and Mark D. Zoback. 1989. Global patterns of tectonic stress. *In* Nature, Vol. 341, p. 291-298.

Zoback, Mary Lou. 1992. First- and second-order patterns of stress in the lithosphere; the World Stress Map Project. *In* Journal of Geophysical Research, Solid Earth and Planets. Vol. 97, No. 8. p. 11,703-11,728. American Geophysical Union. Washington, D.C.

Wright, A.C., and P.R. Kyle. 1990. Royal Society Range. *In* McMurdo Volcanic Group-Western Ross Embayment. *In* Volcanoes of the Antarctic Plate and Southern Oceans. Vol. 48. p. 131-139. American Geophysical Union. Washington, D.C.

Wright-Grassham, Anne C. 1988. Volcanic geology, mineralogy, and petrogenesis of the Discovery volcanic subprovince, southern Victoria Land, Australia. New Mexico Institute of Mining and Technology. Socorro, NM.

WSM. World Stress Map Project. http://www.world-stress-map.org/

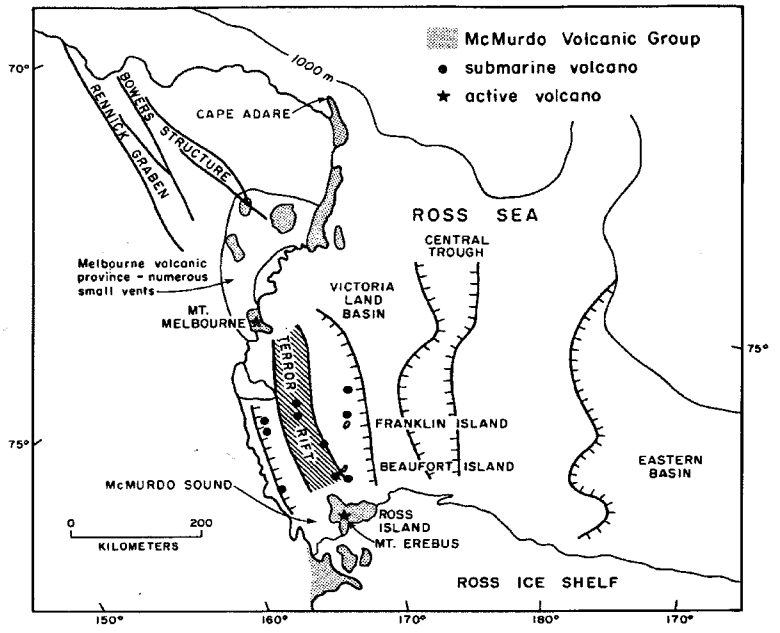

Fig. A.I. Simplified tectonic map of the western Ross Embayment, based on work by *Kyle and Cole* [1974], *Cooper et al.* [1987], *Gair et al.* [1969], *Warren* [1969], and *Wright-Grassham* [1987], showing the distribution of McMurdo Volcanic Group rocks along the western margin of the Ross Embayment.

Figure 1 (Kyle, 1990)

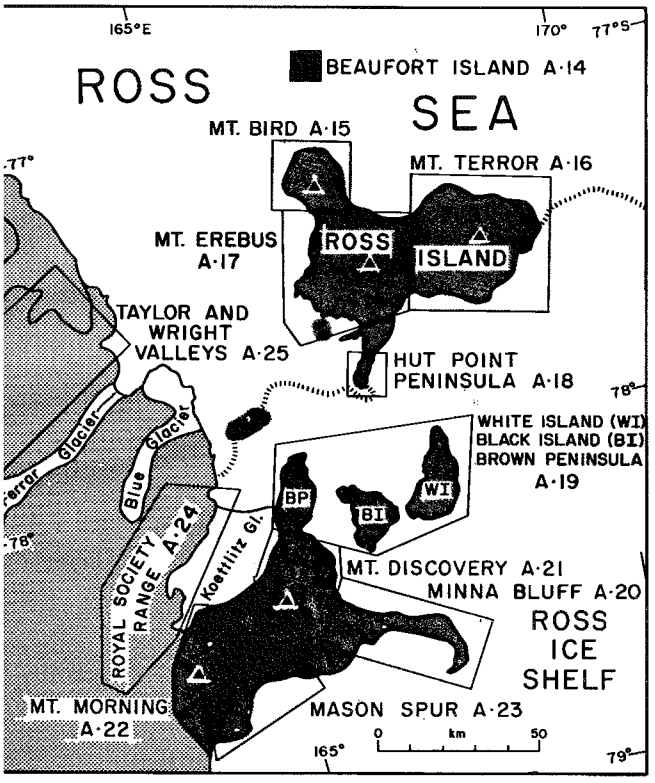

Fig. A.III.1. Generalized distribution of volcanic rocks in Erebus volcanic province, showing the location of the individual volcanic centers described, as indicated, by name and IVD number.

Figure 2 (Kyle, 1990)

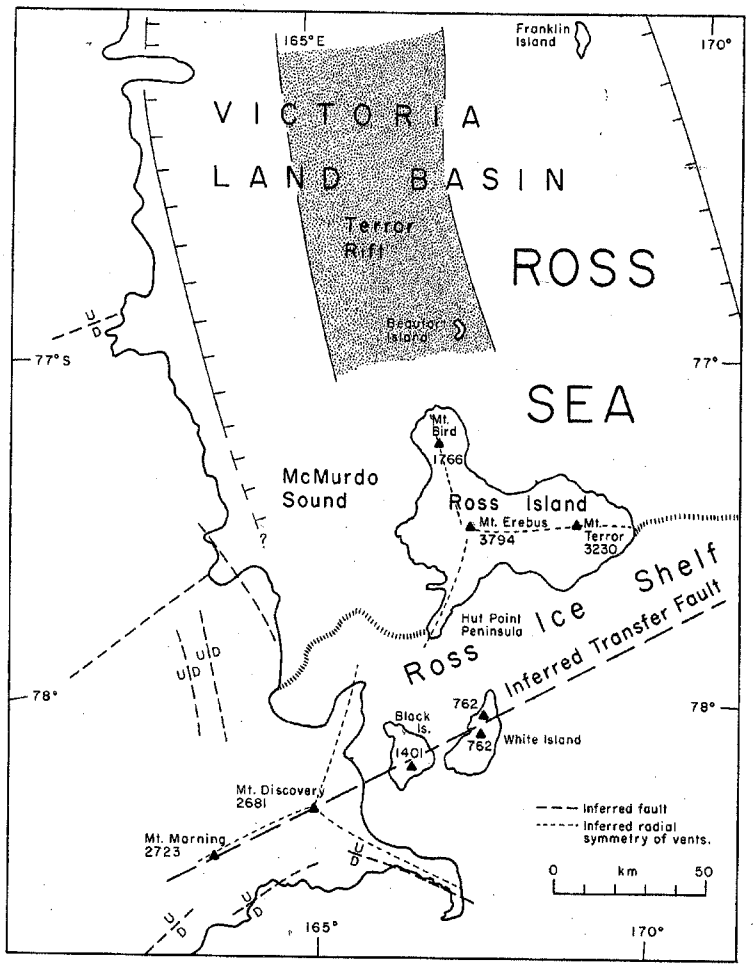

Fig. A.III.4. Generalized tectonic map of Erebus volcanic province, compiled from *Warren* [1969], *Cooper et al.* [1987], *Wright-Grassham* [1987], and Kyle (unpublished observations, 1987).

Figure 3 (Kyle, 1990)

Fig. A.24.1. Geologic map of McMurdo Volcanic Group rocks exposed in the foothills of the Royal Society Range [after *Blank et al.*, 1963; *Keys et al.*, 1977; *Skinner et al.*, 1976; *Wright*, 1980]. Encircled numbers refer to the location of analyzed samples cited in Table A.24.1; boxed numbers refer to K-Ar ages in millions of years.

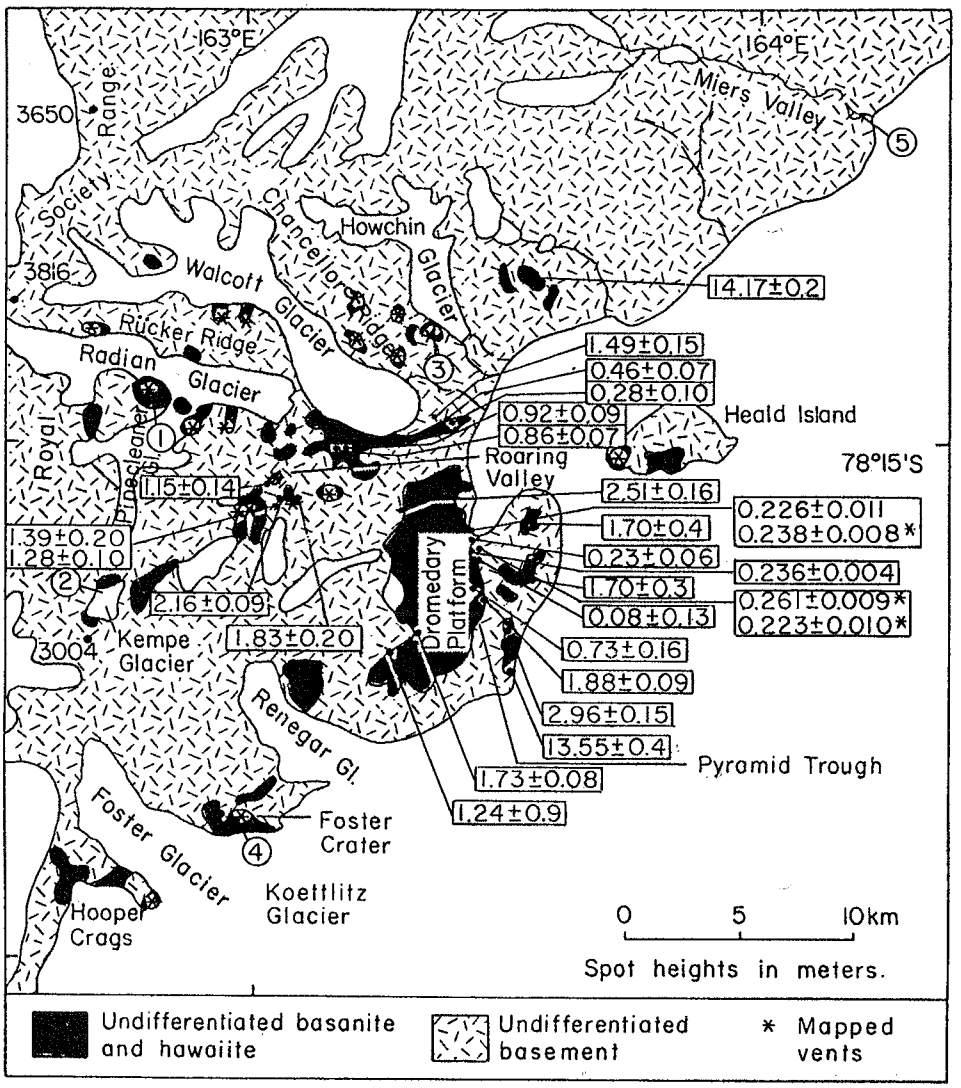

Figure 4 (Wright and Kyle, 1990)

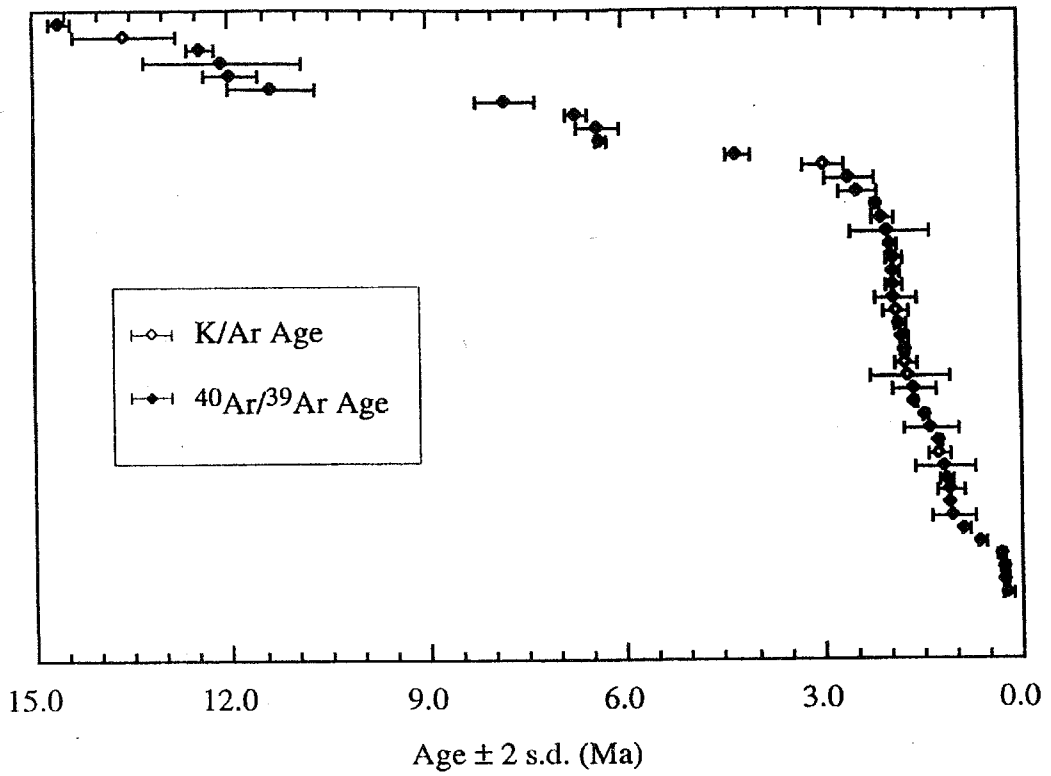

Figure 5. Plot of Royal Society Range eruption ages (from table 3) showing pulses of volcanism from 15 to 4. 3 Ma and continuous volcanism since 2.5 Ma.

Figure 5 (Wilch, unpublished report)

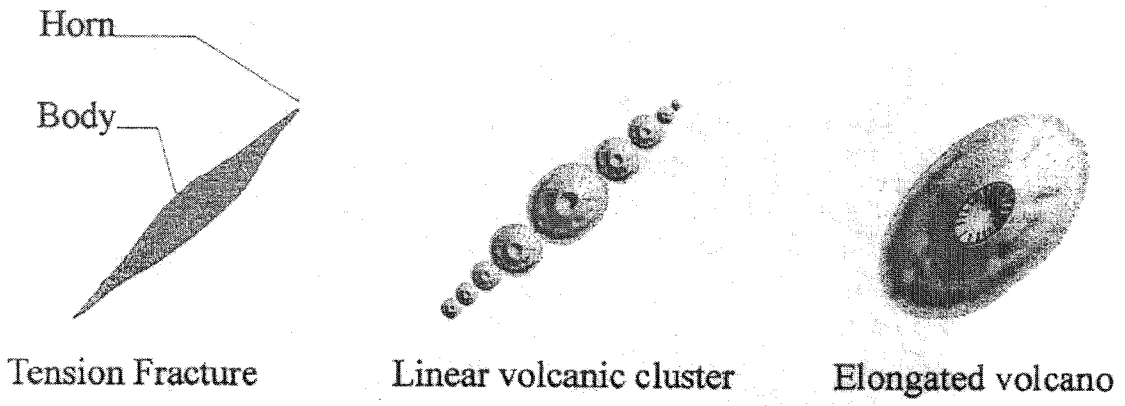

"Original form of a tension crack which can be related to a linear cluster of volcanoes or to an elongated volcano." Adapted from Adiyaman (1998).

Figure 6

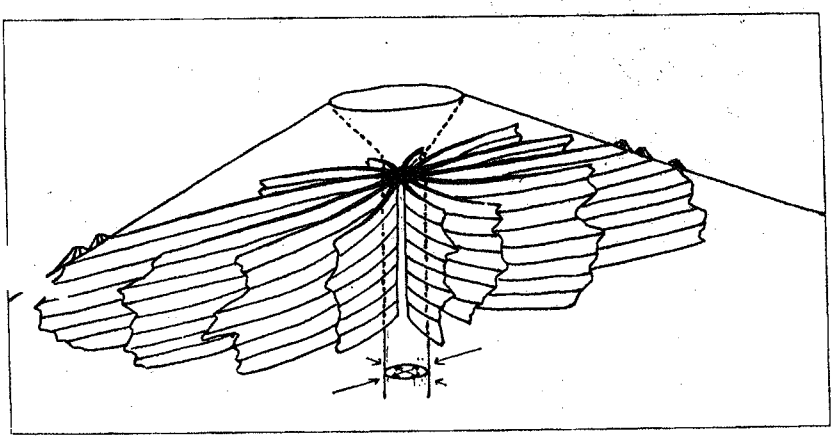

Fig.3. Diagram showing the radial dikes and flank volcanoes of a polygenetic volcano under a differential horizontal stress. The zone of flank volcanoes corresponds to the trend of radial dike concentration; hence to the trend of maximum compression of the horizontal component of the ambient stress. (After Nakamura, 1976.)

Figure 7 (Nakamura, 1977)

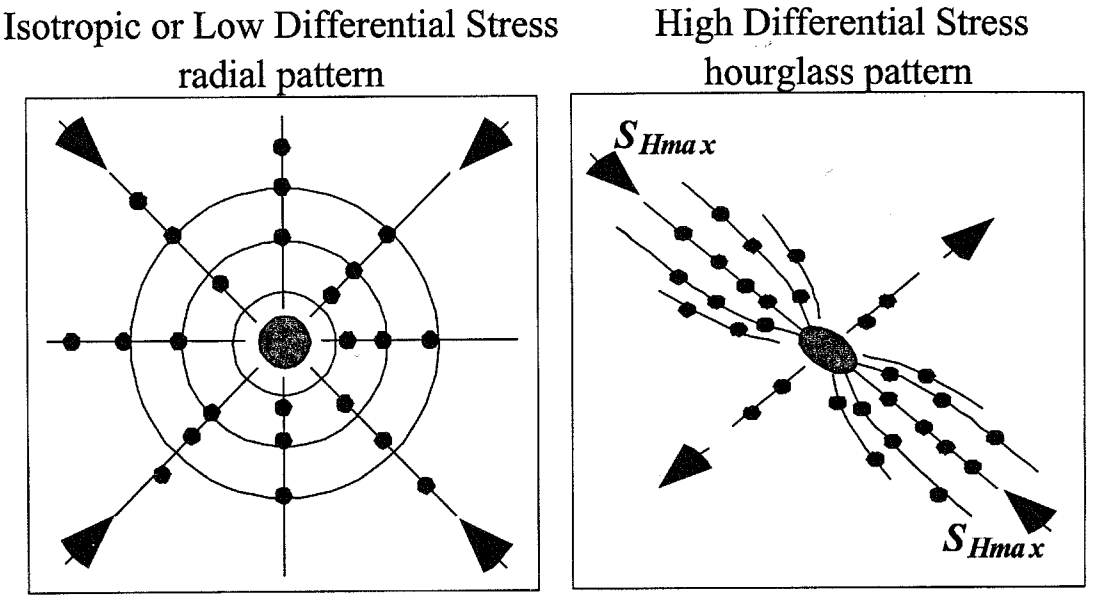

Figure 8 (provided by T. Wilson)

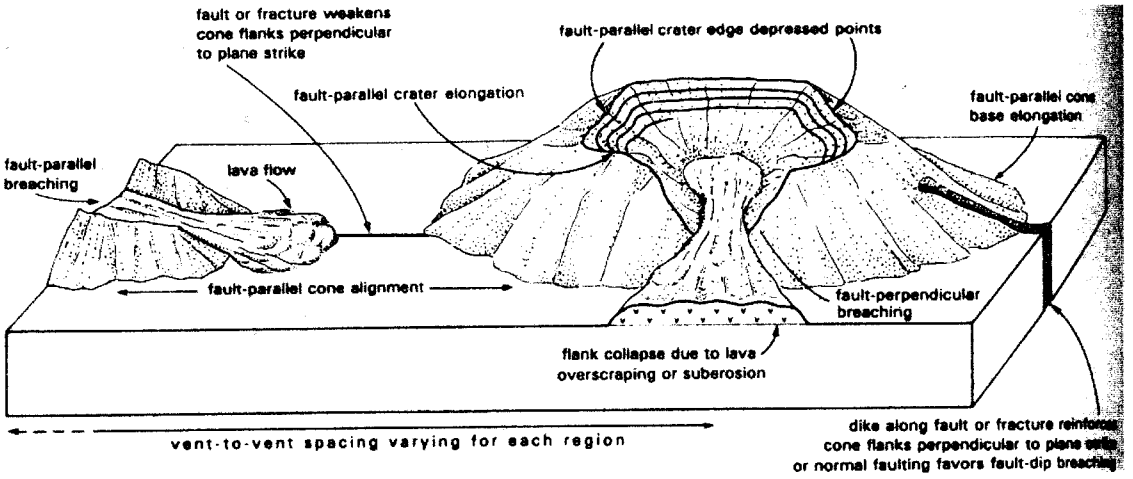

Figure 9 (Tibaldi, 1995)

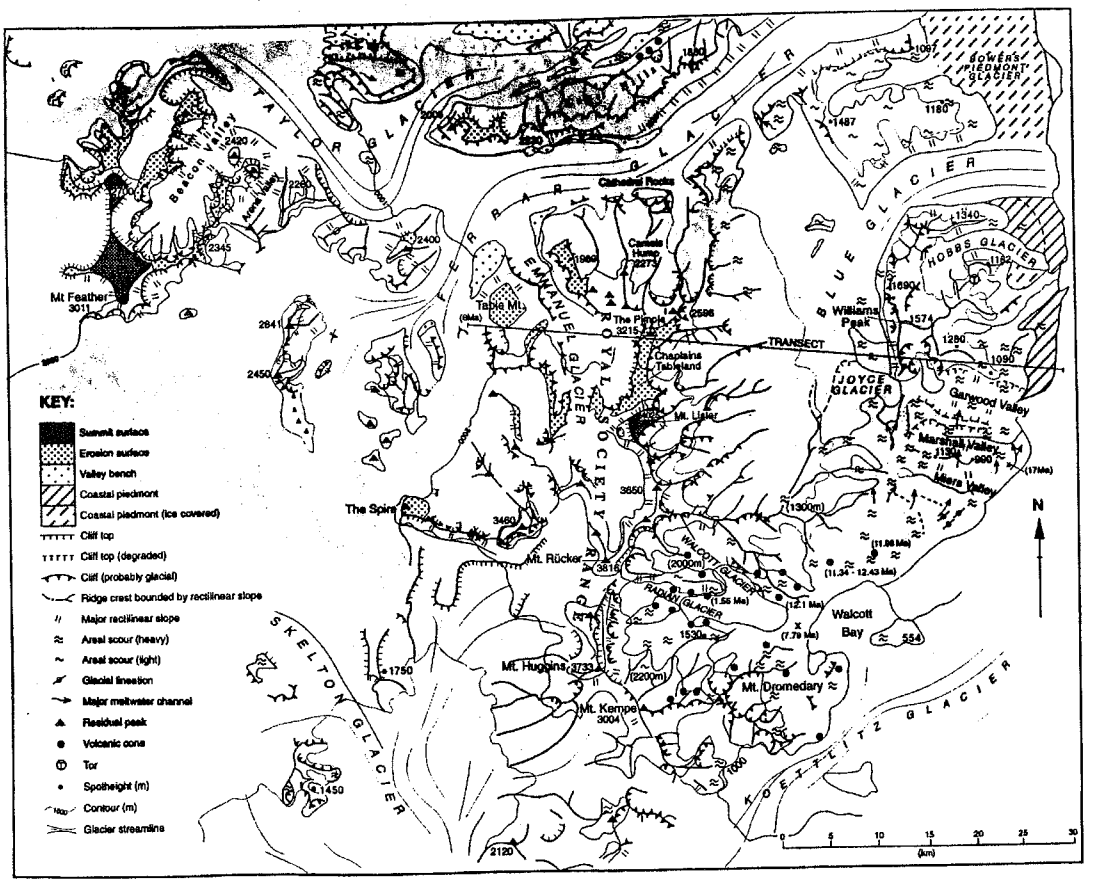

Fig. 4. Geomorphological map compiled from fieldwork, supplemented by air photographs. The transect line shows the location of the cross-section in Fig. 8.

Figure 10 (Sugden, 1999)

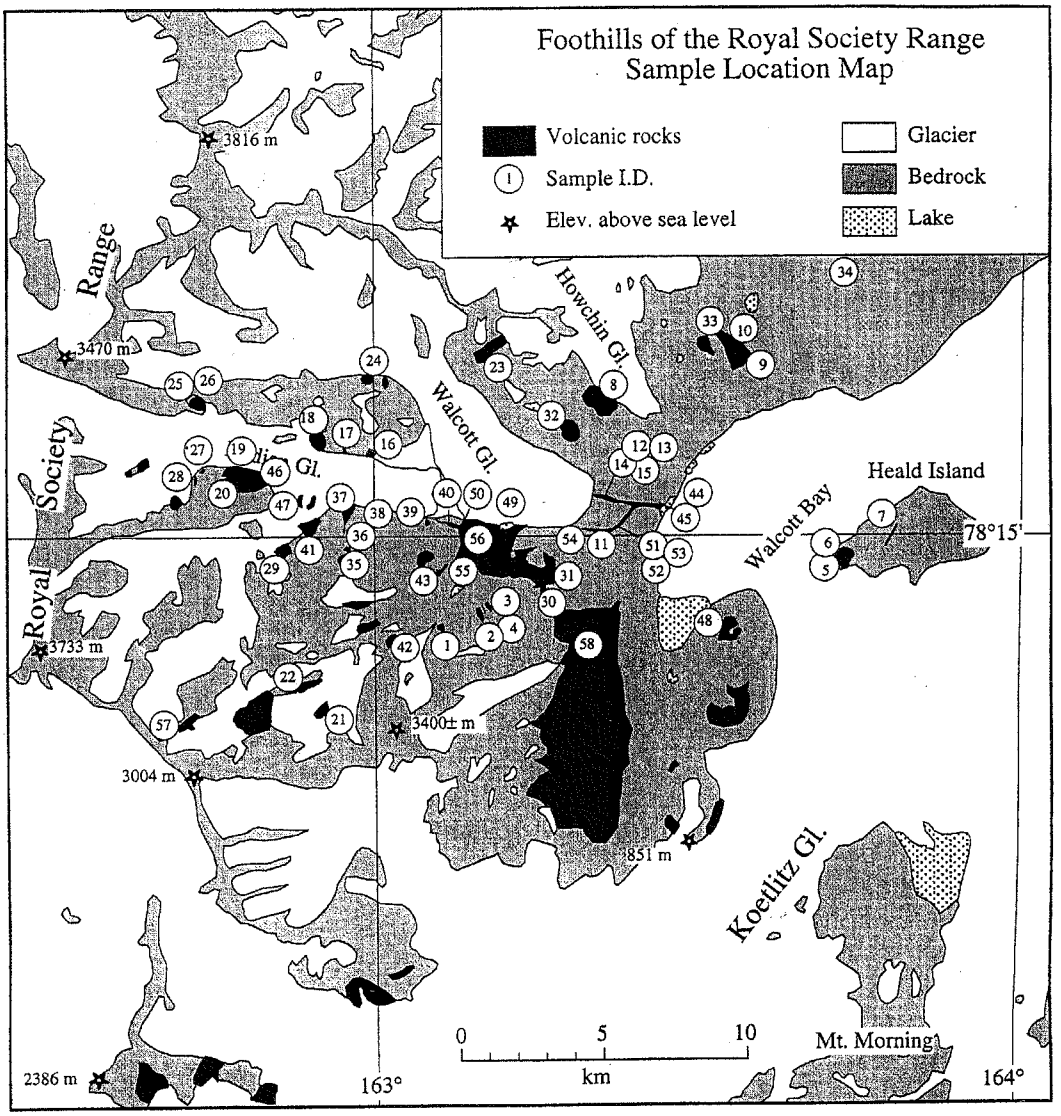

Figure 1. Geologic sketch map showing distribution of sampled basaltic volcanic outcrops in Southern Foothills of the Royal Society Range. Sample numbers shown on map are preceded by TW94- in text and tables. Map is based on 1:250,000 Ross Island and Vicinity topographic map.

Figure 11 (Wilch, unpublished report)

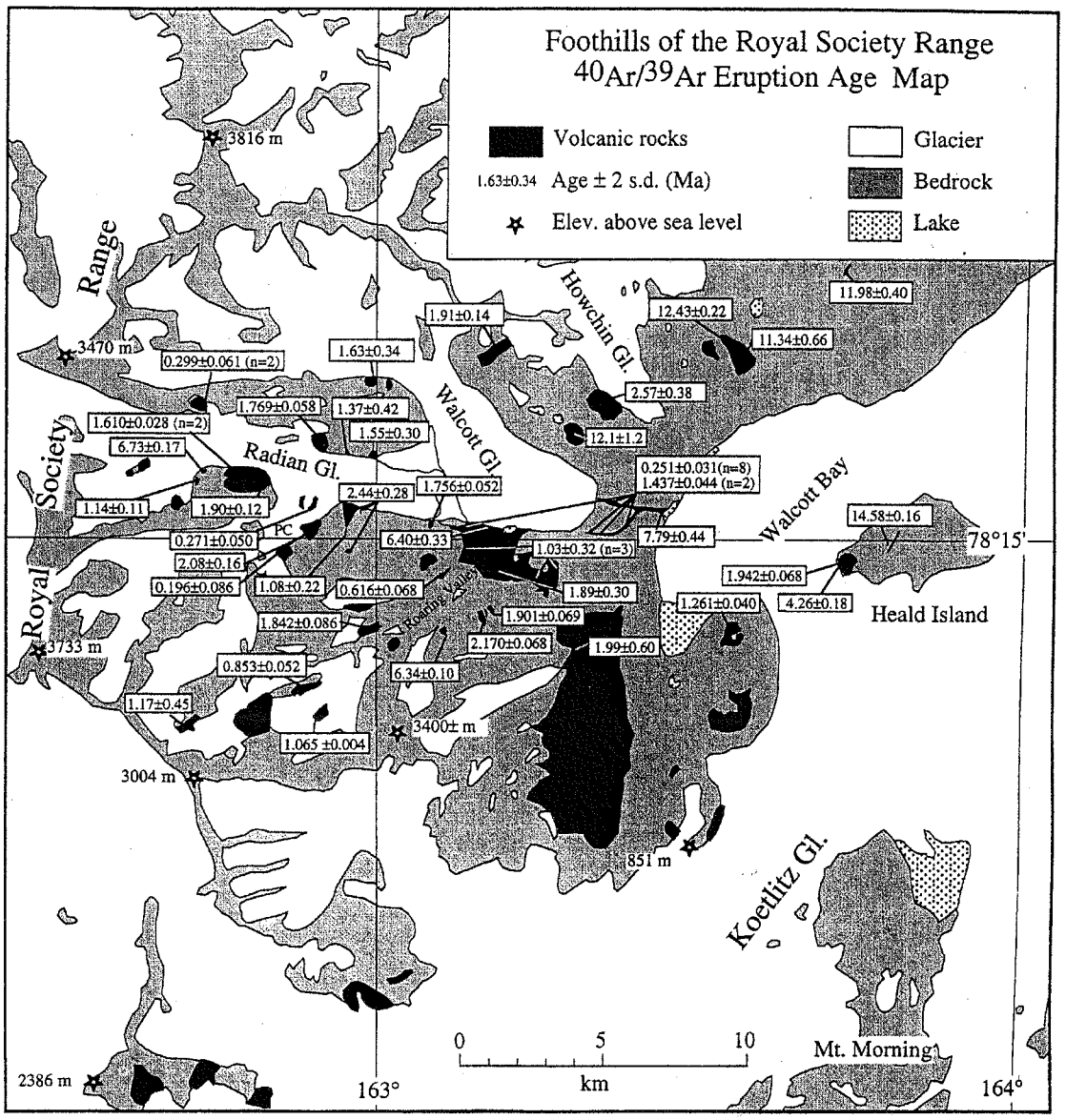

Figure 2. Geologic sketch map showing distribution of basaltic volcanic outcrops in Southern Foothills of the Royal Society Range. $^{40}Ar/^{39}Ar$ eruption ages (± 2 s.d.) are in million of years. Map is based on 1:250,000 Ross Island and Vicinity topographic map.

Figure 12 (Wilch, unpublished report)

Age Data for McMurdo Volcanics - Royal Society Range

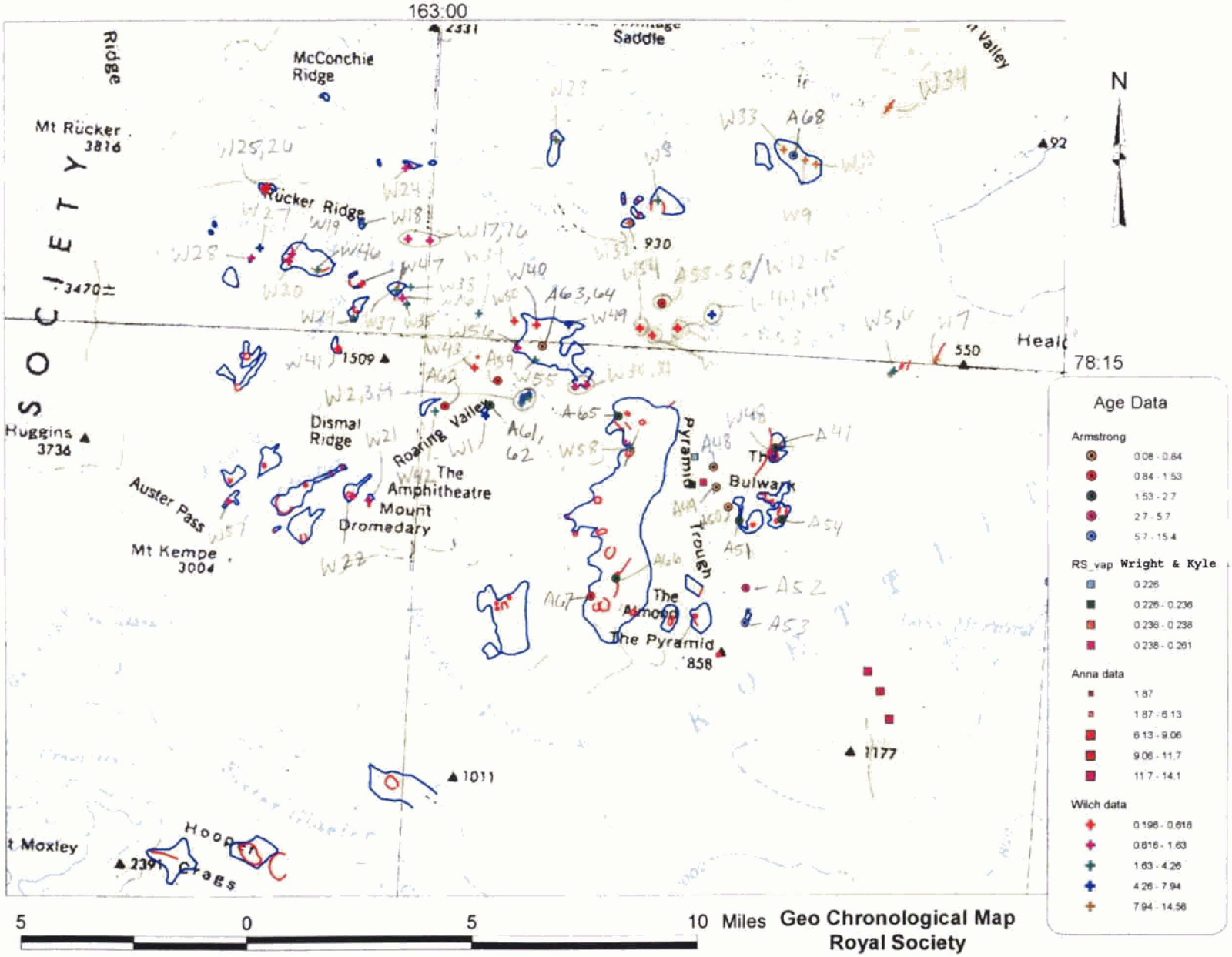

Figure 13
"Working map" showing dikes, elongate cones, circular cones, and Wilch (unpublished report) and Armstrong (1978) dated samples

				CHART 1			
ALIGNMENT ID	DATED BY	TREND	DATE Ma	VARIANCE Ma	INDICATOR	QUALITY	REMARKS
D1	W19	N23E	1.620	0.280	On Dike	Definite	On dike with W20
D1	W20	N23E	1.600	0.250	On Dike	Definite	On dike with W19
D2	W23	N46W	1.910	0.140	On Dike	Definite	
D3	W25	N43W	0.320	0.035	On Dike	Definite	On dike with W26
D3	W26	N43W	0.280	0.130	On Dike	Definite	On dike with W25
D4	W30	N49E	0.981	0.072	On Dike	Definite	On dike with W31
D4	W31	N49E	1.210	0.180	On Dike	Definite	On dike with W30
D5	W37	N14E	2.505	0.064	On Dike	Definite	On dike aligned with cone
D6	W46	N85E	1.900	0.120	On Dike	Definite	
D7	W48	N19E	1.261	0.040	On Dike	Definite	
D7	A47	N19E	1.660	0.400	On Dike	Definite	Match to W48
D8	A54	N17E	1.650	0.300	On Dike	Definite	
D9	W6	N18E	4.260	0.180	On Dike	Definite	
D10	W34	N38E	11.980	0.400	On Dike	Definite	
D11	W7	N26E	14.580	0.160	On Dike	Definite	
EC1	W47	N33E	0.271	0.050	On Elongate Cone	Definite	Near elongate cones with linear trends
EC2	W22	N2E	0.853	0.052	On Elongate Cone	Definite	Near cones with linear trends
EC3	W21	N1E	1.065	0.004	On Elongate Cone	Definite	Near cones with linear trends
EC4	A66	N19E	1.680	0.080	On Elongate Cone	Definite	Next to dike with same trend
EC5	W58	N27E	1.990	0.600	On Elongate Cone	Definite	
EC5	A65	N27E	2.440	0.160	On Elongate Cone	Definite	Match to W58
EC6	W29	N20E	2.080	0.160	On Elongate Cone	Definite	Aligned with W41 cone
EC7	W8	N3W	2.570	0.380	On Elongate Cone	Definite	Also near cones with linear trend
CC1	W41	N20E	0.196	0.086	On Circular Cone	Possible	Poss. Alignment with W29 elongate cone
CC2	W36	N84E	1.080	0.220	On Circular Cone	Possible	In a line of 3 circular cones
CC3	W28	N33E	1.140	0.110	On Circular Cone	Possible	Poss. aligned with lower cone
CC4	W57	N44E	1.170	0.450	On Circular Cone	Possible	Aligned with cones with linear trend
CC5	W16	N75W	1.550	0.300	On Circular Cone	Possible	Aligned with W17
CC5	W17	N75W	1.370	0.420	On Circular Cone	Possible	Aligned with W16
CC5	W18	N75W	1.769	0.058	On Circular Cone	Possible	Possible alignment with W16 & W17
CC6	W24	N83W	1.630	0.340	On Circular Cone	Possible	Poss. Alignment with cone to the left
CC7	W2	N58E	2.170	0.068	On Circular Cone	Possible	Linear alignment with W3 & W4
CC7	W3	N58E	1.925	0.094	On Circular Cone	Possible	Linear alignment with W2 & W4
CC7	W4	N58E	1.877	0.082	On Circular Cone	Possible	Linear alignment with W2 & W3
CC8	W35	N14E	2.534	0.054	On Circular Cone	Probable	Aligned with W38 & near linear dike
CC8	W38	N14E	2.280	0.240	On Circular Cone	Probable	Aligned with W35 & near linear dike
CC9	W10	N66W	11.340	0.660	On Circular Cone	Probable	Aligned with W33
CC9	W33	N66W	12.430	0.220	On Circular Cone	Probable	Aligned with W10
CC10	W32	N21E	12.100	1.200	On Circular Cone	Possible	Aligned with 2 cones with linear trend
D = DIKE / EC = ELONGATE CONE / CC = CIRCULAR CONE							

APPENDIX A

Armstrong (1978) Data Chart

PID	X	Y	K	AR	DATE	VAR	NAME	REMARKS	RECALC	RECALC	X_COORD	Y_COORD
0	1090358.6345	920146.7309	4.210	2.6400	15.40	0.50	MM32		15.8066	0.0000	1090358.634500	920146.730900
1	1078753.4011	902376.7072	4.600	0.2100	1.15	0.02	MM106		1.1808	0.0000	1078753.401100	902376.707200
2	1112447.9659	912848.7575	1.270	0.2650	5.30	0.14	15170	Match Ann ID 4753 ???	5.1900	0.3200	1112447.965900	912848.757500
3	1123934.1041	943577.2755	3.340	0.3640	2.70	0.09	21001	Match Kyle ID 34	2.7700	0.0900	1123934.104100	943577.275500
4	1125502.3839	939788.4558	3.660	0.3260	2.25	0.05	21047	Match Kyle ID 35	2.3100	0.0500	1125502.383900	939788.455800
5	1124162.5115	937858.1433	1.470	0.1390	2.20	0.09	21094	Match Kyle ID 30	2.2600	0.0900	1124162.511500	937858.143300
6	1120937.9868	940083.3786	1.930	0.1660	2.10	0.40	21068	Match Kyle ID 32	2.1600	0.4000	1120937.986800	940083.378600
7	1144582.0362	934060.6280	1.810	0.7570	10.90	0.40	21230	Match Kyle ID 26	11.1000	0.4000	1146033.383631	934201.080977
8	1146360.4035	926193.6894	4.330	0.6490	3.80	0.09	21205	Match Kyle ID 29	3.9000	0.0900	1146360.403500	926193.689400
9	1146763.7241	926211.5342	1.880	0.2550	3.35	0.14	21208	Match Kyle ID 27	3.4400	0.7400	1146763.724100	926211.534200
10	1164734.2194	1029205.8240	3.660	0.6460	4.50	0.60	15970	Match Kyle ID 16	4.6200	0.6000	1164734.219400	1029205.824000
11	1156589.2125	1033863.3391	1.040	0.1610	3.70	0.20	PKA29(=22932)	Match Kyle ID 17	3.8000	0.2000	1156589.212500	1033863.339100
12	1155578.9700	1031914.8865	2.940	0.3420	3.00	0.15	PKA31(=22934)	Match Kyle ID 18	3.0800	0.1500	1155578.970000	1031914.886500
13	1155829.1837	1030234.7244	4.720	0.6040	3.15	0.09	PKA32(=22935)	Match Kyle ID 19	3.2300	0.0900	1155829.183700	1030234.724400
14	1222441.6732	1000625.7359	4.520	0.2440	1.31	0.04	PKA40(=22934)	Match Kyle ID 5	1.3500	0.0400	1222135.724450	1000702.223088
15	1223926.7176	994800.1602	4.840	0.2410	1.29	0.05	PKA52(=22955)	Match Kyle ID 3	1.3200	0.0500	1224181.674892	995182.596138
16	1224680.3319	1001964.1925	1.250	0.0344	0.80	0.14	PKA73(=22976)	Match Kyle ID 2	0.8200	0.1400	1224144.921587	1000944.363333
17	1150599.8138	1000737.6404	2.340	0.0972	0.94	0.05	PKA7(=22910)	Match Kyle ID 9	0.9400	0.0500	1149650.852857	997471.024845
18	1150549.9709	1000711.8122	1.740	0.0608	0.80	0.20	PKA6(=22909)	Match Kyle ID 8	0.8000	0.2000	1150595.594022	997235.330283
19	1191278.1309	999616.7990	1.500	0.0640	0.80	0.50	14970	Match Kyle ID 6	0.8200	0.5000	1191278.130900	999616.799000
20	1158537.4373	971745.4149	1.510	0.0538	1.00	0.15	HP4(=22878)	Match Kyle ID 22 ???	1.1800	0.0000	1158517.536691	970684.049113
21	1156159.7248	968304.6297	1.680	0.0334	0.57	0.03	HP26(=22900)		0.5853	0.0000	1156020.420540	967455.537070
22	1156520.3856	968294.6522	1.420	0.0199	0.43	0.07	HP18(=22892)		0.4415	0.0000	1156241.777081	967452.193106
23	1171748.9982	1001895.7274	1.590	0.0300	0.55	0.15	13170	Match Kyle ID 14	0.5500	0.1500	1172329.132006	1000670.600107
24	1171748.9982	1001895.7274	2.670	0.0401	0.44	0.09	E S		0.4518	0.0000	1172329.132006	1000674.203422
25	1171144.8144	1000376.6167	4.040	0.0198	0.15	0.05	E 15		0.1540	0.0000	1170779.871465	1003182.645832
26	1173404.4985	1005628.2450	3.450	0.1100	0.81	0.02	E 10	Match Kyle ID 12	0.8100	0.0200	1172548.792830	1005891.539052
27	1174569.8471	1005359.1135	2.570	0.0802	0.73	0.07	E 11	Match Kyle ID 13	0.7300	0.0700	1173084.116377	1005584.794116
28	1051922.9333	1011509.5788	1.440	0.2370	3.75	0.20	WV3		3.8505	0.0000	1051922.933300	1011509.578800
29	1058054.9555	1015118.5896	1.080	0.1450	3.50	0.20	WV 2E		3.5938	0.0000	1058054.955500	1015118.589600
30	1064241.6154	990704.9488	1.180	0.1310	2.93	0.10	1		3.0085	0.0000	1064241.615400	990704.948800
31	1064269.7107	992317.5740	1.200	0.1440	2.89	0.10	3		2.9675	0.0000	1064269.710700	992317.574000
32	1063535.3191	992475.4040	1.180	0.1350	2.87	0.15	6		2.9469	0.0000	1063535.319100	992475.404000
33	1062552.7896	988888.7323	1.500	0.2760	4.64	0.12	7		4.7644	0.0000	1062552.789600	988888.732300
34	1062564.5777	988857.1660	1.520	0.2890	4.50	0.70	8		4.6202	0.0000	1062564.577700	988857.166000
35	1061027.1638	990694.4526	1.360	0.1580	3.00	0.10	10		3.0804	0.0000	1061027.163800	990694.452600
36	1060682.6255	990678.4858	1.270	0.1350	2.66	0.06	10'		2.7313	0.0000	1060682.625500	990678.485800
37	1060506.1938	987086.3033	0.906	0.1070	3.11	0.09	12		3.1933	0.0000	1060506.193800	987086.303300
38	1060866.8771	987039.4989	0.843	0.0990	2.95	0.07	13		3.0291	0.0000	1060866.877100	987039.498900
39	1056379.1130	992814.3352	0.979	0.1320	3.33	0.10	16		3.4192	0.0000	1056379.113000	992814.335200
40	1057549.2371	992611.3561	0.968	0.1320	3.38	0.14	19		3.4706	0.0000	1057549.237100	992611.356100

41	1053623.3754	992767.9494	1.030	0.0770	2.00	0.18	20		2.0536	0.0000	1053623.375400	992767.949400
42	1053545.8011	991095.4809	0.972	0.0710	1.79	0.13	23		1.8380	0.0000	1053545.801100	991095.480900
43	1053354.3206	987317.5672	1.440	0.1110	1.94	0.12	24		1.9920	0.0000	1053354.320600	987317.567200
44	1050123.1647	983839.1814	1.470	0.1070	1.84	0.11	26		1.8893	0.0000	1050123.164700	983839.181400
45	1050541.9696	985406.2112	1.250	0.0720	1.53	0.06	27		1.5710	0.0000	1050541.969600	985406.211200
46	1050482.1005	983764.0939	1.370	0.1130	2.00	0.06	29		2.0536	0.0000	1050482.100500	983764.093900
47	1080549.6626	926248.0843	0.880	0.0630	1.66	0.40	30	Match to Wilch TW94-48	1.7000	0.4000	1080623.557128	924954.930066
48	1078212.8784	924648.5512	1.110	0.0070	0.22	0.12	31a		0.2259	0.0000	1078422.246228	924266.762807
49	1078211.8592	924524.3743	1.150	0.0050	0.08	0.13	32		0.0800	0.1300	1078519.753065	923539.113931
50	1078069.2864	922855.5970	0.812	0.0230	0.71	0.16	33		0.7300	0.1600	1078943.704977	922830.965491
51	1078462.9619	922801.2619	0.799	0.0570	1.83	0.09	35		1.8800	0.0900	1079337.380477	922345.578979
52	1079190.0377	922633.7209	1.200	0.1330	2.88	0.15	36		2.9600	0.1500	1079559.510338	919936.570641
53	1079355.2163	918989.6797	0.996	0.5470	13.20	0.40	37		13.5500	0.4000	1079539.952619	918694.101589
54	1080726.6064	922727.2641	0.612	0.0370	1.65	0.30	40		1.7000	0.3000	1080849.763946	922394.738726
55	1077409.7663	930255.0017	0.405	0.0850	5.70	0.50	43	Match to Wilch TW94-13	5.8516	0.0000	1076581.288657	930149.470873
56	1077037.2912	930276.6100	1.150	0.0190	0.45	0.07	44	Match to Wilch TW94-15	0.4621	0.0000	1076581.203947	930151.671205
57	1076633.2437	930299.9317	1.190	0.0110	0.27	0.10	45	Match to Wilch TW94-12	0.2772	0.0000	1076579.871787	930155.584936
58	1076601.6772	930301.7485	0.619	0.0360	1.45	0.15	46	Match to Wilch TW94-14	1.4900	0.1500	1076582.269232	930151.336746
59	1070734.0256	927024.7669	0.958	0.0460	1.12	0.14	47a	Match to Wilch TW94-02	1.1500	0.1400	1070758.657109	927381.923784
60	1070392.3026	927011.8767	0.978	0.0420	1.25	0.10	48a	Match to Wilch TW94-01	1.2800	0.1000	1068877.464783	926469.983497
61	1071143.3771	927002.8986	0.840	0.0720	2.10	0.09	49a	Match to Wilch TW94-03	2.1600	0.0900	1070453.694842	926510.268416
62	1071162.2700	927001.8863	0.862	0.0550	1.78	0.19	49b	Match to Wilch TW94-04	1.8300	0.1900	1070472.587742	926509.256116
63	1072349.0146	928614.5052	1.240	0.0390	0.90	0.09	50a	Match to Wilch TW94-56	0.9000	0.0900	1072349.014600	928614.505200
64	1072342.7093	928614.8483	1.300	0.0390	0.84	0.07	50b	Match to Wilch TW94-56	0.8400	0.0700	1072342.709300	928614.848300
65	1074927.2864	926670.5443	0.770	0.0750	2.44	0.16	63	Match to Wilch TW94-58	2.5100	0.1600	1075038.128191	926104.019588
66	1075002.2696	921200.6699	0.986	0.0640	1.68	0.08	65		1.7300	0.0800	1074953.006582	920301.619814
67	1073476.2424	921131.0929	0.833	0.0420	1.21	0.09	66		1.2400	0.9000	1074079.714376	919665.518102
68	1078467.3173	935752.5294	1.120	0.6330	13.80	0.20	73	Match to Willch TW94-09 &10	14.1700	0.2000	1081238.362087	935420.004026

APPENDIX B

Wright and Kyle (1990) Data Chart

Shape	Id	Age	Error	Method	Remark	X	Y
Point	5	1.35	0.04	K/AR	Kyle	1222146.60	1000791.82
Point	2	0.82	0.14	K/AR	Kyle	1224095.66	1000929.40
Point	3	1.32	0.05	K/AR		1224187.38	995242.73
Point	5	1.75	0.30	K/AR	Topping cone	1221894.37	997558.67
Point	6	0.82	0.50	K/AR	Kyle	1191259.76	999691.17
Point	7	0.86	0.20	K/AR	Kyle	1160993.10	986690.88
Point	8	0.80	0.20	K/AR		1151722.53	996812.37
Point	9	0.94	0.05	K/AR		1150961.18	997887.22
Point	10	0.68	0.14	K/AR		1147915.78	1000887.84
Point	12	0.81	0.02	K/AR		1173398.64	1005635.08
Point	13	0.73	0.07	K/AR		1174518.28	1005366.37
Point	14	0.55	0.15	K/AR		1171831.16	1001649.19
Point	16	4.62	0.60	K/AR		1164755.07	1029147.39
Point	17	3.80	0.20	K/AR		1156559.35	1033849.85
Point	18	3.08	0.15	K/AR		1155484.50	1032013.65
Point	19	3.23	0.09	K/AR		1155798.00	1030267.03
Point	21	1.18	0.00	K/AR	my	1156467.95	965654.35
Point	22	1.18	0.00	K/AR		1158903.78	971112.16
Point	23	0.20	0.10	K/AR		1170932.80	943435.43
Point	26	11.1	0.40	K/AR		1145332.77	934308.46
Point	27	4.41	0.06	K/AR		1153473.90	927884.61
Point	27	3.44	0.74	K/AR		1146763.83	926262.74
Point	29	3.90	0.09	K/AR		1146286.81	926262.74
Point	30	2.26	0.09	K/AR		1124184.92	937902.01
Point	32	2.16	0.40	K/AR		1120972.99	940128.10
Point	34	2.77	0.09	K/AR		1123898.71	943626.24
Point	35	2.31	0.05	K/AR		1125488.77	939778.29

APPENDIX C
Sugden (1999) Data Chart

Shape	ID	Age	Variance	Source	Remarks
Point	1	1.261	0.040		Match to Wilch TW94-48
Point	2	13.550	0.400	WK	Match to Wilch Outcrop
Point	3	1.990	0.600		Match to Wilch TW94-58
Point	4	1.210	0.180		Match to Wilch TW94-31
Point	5	6.340	0.100		Match to Wilch TW95-01
Point	6	1.065	0.004		Match to Wilch TW94-21
Point	7	0.853	0.052		Match to Wilch TW94-22
Point	8	0.000	0.000		Match to Wilch Outcrop
Point	9	1.080	0.220		Match to Wilch TW94-36
Point	10	2.080	0.160		Match to Wilch TW94-29
Point	11	1.900	0.120		Match to Wilch TW94-46
Point	12	1.620	0.280	WI	Match to Wilch TW94-20
Point	13	0.000	0.000		Match to Wilch TW94-18
Point	14	0.000	0.000		Match to Wilch TW94-17
Point	15	1.550	0.300	Sug	Match to Wilch TW94-16
Point	16	1.630	0.340		Match to Wilch TW94-24
Point	17	0.000	0.000		Match to Flow ID 17
Point	18	1.910	0.140		Match to Wilch TW94-23
Point	19	0.000	0.000		No match to Wilch dates?
Point	20	12.100	1.200	Sug	Match to Wilch TW94-32
Point	21	2.570	0.380		Macth to Wilch TW94-08
Point	22	11.340	0.660	Sug	Match to Wilch TW94-10
Point	23	11.980	0.400	Sug	Match to Wilch TW94-34

APPENDIX D

Wilch (unpublished report) Data Chart

ID	DATE_	VARIANC	SAMPLE_I	LOCALITY	METH	COORDINATE	COORDINA_1	X_COORD	Y_COORD
1	6.340	0.100	TW94-01	Roaring Valley	Ar-Ar	1070279.52	925580.55	1070356.800156	926131.171111
2	2.170	0.068	TW94-02	Roaring Valley	Ar-Ar	1071648.15	925863.71	1071628.829961	926588.211462
3	1.925	0.094	TW94-03	Roaring Valley	Ar-Ar	1072025.70	926288.46	1071871.139688	926790.781014
4	1.877	0.082	TW94-04	Roaring Valley	Ar-Ar	1072072.90	926099.68	1071754.119357	926824.181462
5	1.942	0.068	TW94-05	Heald Island	Ar-Ar	1084390.52	927421.11	1084863.860955	927739.890643
6	4.260	0.180	TW94-06	Heald Island	Ar-Ar	1084437.71	927090.75	1084766.150663	927651.031131
7	14.580	0.160	TW94-07	Heald Island	Ar-Ar	1085947.92	927987.44	1086346.395804	928132.340292
8	2.570	0.380	TW94-08	Howchin Glacier	Ar-Ar	1076650.71	933461.94	1076457.509610	933824.190731
9	10.500	1.100	TW94-09	Howchin Glacier	Ar-Ar	1082030.82	934405.82	1081668.569269	935263.146730
10	11.340	0.660	TW94-10	Howchin Glacier	Ar-Ar	1081653.27	934972.14	1082063.820828	935117.040292
11	0.243	0.034	TW94-11	Walcott Glacier	Ar-Ar	1076178.77	928459.38	1076263.295171	929014.831121
12	0.264	0.019	TW94-12	Walcott Glacier	Ar-Ar	1076792.29	929875.20	1076584.969622	930151.075355
13	1.421	0.030	TW94-13	Walcott Glacier	Ar-Ar	1077075.45	929828.00	1076585.145583	930150.909523
14	1.452	0.022	TW94-14	Walcott Glacier	Ar-Ar	1076320.35	929969.58	1076585.221502	930150.218469
15	0.244	0.024	TW94-15	Walcott Glacier	Ar-Ar	1076556.32	929969.58	1076586.507561	930150.705365
16	1.550	0.300	TW94-16	Radian Glacier	Ar-Ar	1068250.18	931951.73	1068368.524667	932417.712126
17	1.370	0.420	TW94-17	Radian Glacier	Ar-Ar	1067353.50	932046.12	1067597.585876	932467.722876
18	1.769	0.058	TW94-18	Radian Glacier	Ar-Ar	1066220.84	932659.64	1066013.736833	933014.674001
19	1.620	0.280	TW94-19	Radian Glacier	Ar-Ar	1063483.59	931951.73	1063483.590000	931951.730000
20	1.600	0.250	TW94-20	Radian Glacier	Ar-Ar	1063342.01	931149.43	1063364.199625	931696.774085
21	1.065	0.004	TW94-21	Roaring Valley	Ar-Ar	1065701.71	922796.10	1066184.710975	923124.540663
22	0.853	0.052	TW94-22	Roaring Valley	Ar-Ar	1065324.16	924023.15	1065623.620604	923250.348441
23	1.910	0.140	TW94-23	Walcott Glacier	Ar-Ar	1072828.00	935396.89	1072828.000000	936000.641218
24	1.630	0.340	TW94-24	Walcott Glacier	Ar-Ar	1068391.77	934688.98	1067511.581539	934999.634751
25	0.320	0.035	TW94-25	Radian Glacier	Ar-Ar	1062020.58	934169.85	1062523.544835	934221.625792
26	0.280	0.130	TW94-26	Radian Glacier	Ar-Ar	1062492.52	934217.04	1062573.881959	934357.574292
27	6.730	0.170	TW94-27	Radian Glacier	Ar-Ar	1062303.75	931762.96	1062333.336167	932162.373251
28	1.140	0.110	TW94-28	Radian Glacier	Ar-Ar	1061784.61	931385.40	1062036.092417	931799.606334
29	2.080	0.160	TW94-29	Radian-Pipecleaner Glacier	Ar-Ar	1065701.71	929308.87	1065655.481614	929641.714376
30	0.981	0.072	TW94-30	Roaring Valley	Ar-Ar	1073677.49	927373.92	1073522.929688	927171.059591
31	1.210	0.180	TW94-31	Roaring Valley	Ar-Ar	1074385.40	927704.28	1073912.059045	927221.279025
32	12.100	1.200	TW94-32	Walcott Glacier	Ar-Ar	1075234.89	932329.28	1075428.090390	933029.631413
33	12.430	0.220	TW94-33	Howchin Glacier	Ar-Ar	1080850.97	935444.08	1080911.345122	935637.280390
34	11.980	0.400	TW94-34	Walcott Galcier	Ar-Ar	1085145.62	937331.84	1084662.619025	937174.864683
35	2.534	0.054	TW94-35	Radian Glacier	Ar-Ar	1067164.72	928789.74	1067543.792761	930130.363181
36	1.080	0.220	TW94-36	Radian Glacier	Ar-Ar	1067117.53	929356.06	1067385.654636	930363.838805

37	2.505	0.064	TW94-37	Radian Glacier	Ar-Ar	1067731.05	930111.17	1067176.309374	930647.419272
38	2.280	0.240	TW94-38	Radian Glacier	Ar-Ar	1068297.38	929969.58	1067687.165311	930746.216877
39	1.756	0.052	TW94-39	Radian Glacier	Ar-Ar	1070090.75	929450.45	1070100.410019	929817.530741
40	0.247	0.026	TW94-40	Walcott Glacier-Roaring Valley	Ar-Ar	1070704.27	929356.06	1072153.272924	929394.700078
41	0.196	0.086	TW94-41	Pipecleaner	Ar-Ar	1064757.83	928600.96	1065105.590702	928562.319922
42	1.842	0.086	TW94-42	Roaring Valley	Ar-Ar	1067731.05	925910.90	1068552.151657	926306.960799
43	0.616	0.068	TW94-43	Roaring Valley	Ar-Ar	1070421.11	927704.28	1069967.089084	927868.500331
44	7.630	0.320	TW94-44	Walcott Glacier	Ar-Ar	1078491.27	929308.87	1078365.689747	929733.910858
45	7.940	0.240	TW94-45	Walcott Glacier	Ar-Ar	1078208.11	929450.45	1078374.141585	929759.570624
46	1.900	0.120	TW94-46	Radian-Pipecleaner Glacier	Ar-Ar	1064238.70	930960.66	1064379.234292	931382.262876
47	0.271	0.050	TW94-47	Radian-Pipecleaner Glacier	Ar-Ar	1065843.29	930252.75	1065946.841584	930874.059502
48	1.261	0.040	TW94-48	Bulwark	Ar-Ar	1080331.84	925108.61	1080486.400312	924828.469435
49	6.400	0.330	TW94-49	Roaring Valley	Ar-Ar	1072072.90	929261.68	1073299.722476	929406.580292
50	0.242	0.046	TW94-50	Walcott Glacier-Roaring Valley	Ar-Ar	1071364.94	929544.84	1071364.940000	929544.840000
51	1.380	0.160	TW94-51	Walcott Glacier	Ar-Ar	1076981.07	929025.71	1077154.950351	929267.210487
52	0.248	0.036	TW94-52	Walcott Glacier	Ar-Ar	1077122.65	928978.51	1077161.290078	929277.970604
53	0.236	0.022	TW94-53	Walcott Glacier	Ar-Ar	1076981.07	928789.74	1077164.610370	929263.080955
54	0.283	0.024	TW94-54	Walcott Glacier	Ar-Ar	1075565.25	928931.32	1075830.900536	929269.420682
55	1.890	0.300	TW94-55	Roaring Valley	Ar-Ar	1072403.25	927609.89	1072094.129376	928131.531053
56	0.900	0.130	TW94-56	Roaring Valley	Ar-Ar	1071364.99	928506.57	1071480.910234	928574.190136
57	1.170	0.450	TW94-57	Mt. Kemp	Ar-Ar	1060982.32	922937.69	1061194.840429	923092.250312
58	1.990	0.600	TW94-58	Dromedary Platform	Ar-Ar	1074857.34	925014.22	1075504.561306	924965.919903
0	0.000	0.000				0.00	0.00	0.000000	0.000000